

Electrometry of a single resonator mode at a Rydberg-atom–superconducting-circuit interfaceD. M. Walker, L. L. Brown, and S. D. Hogan *Department of Physics and Astronomy, University College London, Gower Street, London WC1E 6BT, UK*

(Received 3 November 2021; accepted 16 February 2022; published 28 February 2022)

The electric-field distribution in a single mode of a $\lambda/4$ superconducting coplanar waveguide (CPW) microwave resonator has been probed using beams of helium Rydberg atoms. In the experiments the atoms were prepared in the $1s55s^3S_1$ Rydberg level by laser photoexcitation. They then traveled over the CPW resonator that was fabricated on a NbN superconducting chip operated at 3.8 K. The resonator was driven at its third-harmonic frequency, near resonant with the two-photon $1s55s^3S_1 \rightarrow 1s56s^3S_1$ transition at $\omega_{55s,56s}/2 = 2\pi \times 19.556499$ GHz. The coherence times of the atom–resonator-field interaction were determined at selected locations above the resonator by time-domain measurements of Rabi oscillations and found to be up to $0.8 \mu\text{s}$ for Rabi frequencies of $\sim 2\pi \times 3$ MHz. The coherence times of the atomic superposition states, generated following the interaction of the atoms with the microwave field in the resonator, were inferred from high-resolution cavity-enhanced Ramsey spectra to be $\sim 2.5 \mu\text{s}$. These Ramsey spectra also allowed the measurement of residual uncanceled dc electric fields of 26.6 ± 0.6 mV/cm at the position of the atoms $\sim 300 \mu\text{m}$ above the surface of the superconducting chip. These results represent an essential step toward applications of hybrid systems, comprising Rydberg atoms coherently coupled to superconducting microwave circuits, in quantum optics and quantum information processing.

DOI: [10.1103/PhysRevA.105.022626](https://doi.org/10.1103/PhysRevA.105.022626)**I. INTRODUCTION**

Transitions between Rydberg states with high principal quantum number n occur at microwave frequencies and exhibit electric dipole transition moments in excess of $1000 e a_0$ for values of $n \gtrsim 30$ [1]. States with these values of n have lifetimes $> 10 \mu\text{s}$. These characteristics make Rydberg states ideally suited to microwave cavity quantum-electrodynamics (QED) experiments [2,3]. They were exploited, for example, in the first observation of modified spontaneous emission in a cavity [4], the first observation of vacuum Rabi oscillations [5], and seminal work on quantum nondemolition photon detection [6].

Microwave cavity QED with two-dimensional chip-based coplanar waveguide (CPW) resonators [7], rather than the three-dimensional cavities used in early experiments, has played a central role in the development of approaches to quantum information processing in superconducting circuits [8]. CPW microwave resonators are scalable, and their small mode volumes allow the generation of strong microwave fields and hence high single-photon Rabi frequencies—typically in excess of 10 MHz [7]. The development of hybrid interfaces between gas-phase Rydberg atoms and these chip-based superconducting circuits [9,10] offers a range of new opportunities in quantum optics and for quantum information processing. These include, for example, optical-to-microwave photon transduction [11–14], hybrid quantum memories [15,16], quantum gates [17–19], and quantum sensors [6,20]. They also have the potential to allow access to previously unexplored regimes of quantum optics [21].

The major challenges in the experimental realization of hybrid interfaces between Rydberg atoms and superconducting circuits center around controlling and minimizing effects of stray electric fields on the atoms located $\sim 100 \mu\text{m}$ from the surfaces of cryogenically cooled superconducting chips [10,22–28]. Recently, significant progress has been made in overcoming these challenges, for example, through the choice of atom, CPW resonator geometry, and quantum states used in the experiments [29]. In experiments with helium Rydberg atoms and niobium nitride (NbN) superconducting CPW resonators with a $\lambda/4$ geometry, coherence times of the atom–resonator-field interactions of ~ 800 ns have been achieved, and cavity-enhanced Ramsey spectroscopy has been performed to exploit the atoms to coherently probe the spectral characteristics of a single resonator mode [29,30]. Experiments have also been performed with magnetically trapped rubidium atoms, photoexcited to Rydberg states close to a superconducting atom chip containing a CPW resonator [31].

In the work reported here, the microwave field distribution in the third-harmonic mode of a $\lambda/4$ CPW resonator was mapped by time-domain measurements of the population transfer between Rydberg states in helium as the atoms traveled across the resonator. From the results of these measurements, effects of the inhomogeneity in the microwave field distribution on the coherence time of the atom–resonator-field interaction were identified. Two-photon Ramsey spectroscopy, in which the enhancement of the microwave field in the CPW resonator is taken advantage of to achieve fast coherent state preparation and manipulation, was performed by injecting pairs of short microwave pulses

into the resonator at times when the atoms were at positions separated by a distance of $\sim\lambda/2$. This is referred to in the following as cavity-enhanced Ramsey spectroscopy. The corresponding spectra were recorded with a free-evolution time of $2\ \mu\text{s}$ and hence intervals between adjacent Ramsey fringes of 250 kHz in the frequency domain. These measurements allowed the average stray dc electric field experienced by the atoms when located above the CPW resonator be determined to a precision of $\pm 0.6\ \text{mV/cm}$ and minimized. This characterization of the spatial distribution of the microwave field in the resonator mode and residual stray dc electric fields above the chip surface pave the way for experiments with dressed states that are expected to allow access to the single-photon strong-coupling regime of this hybrid quantum system.

In the following, the apparatus used in the experiments is described in Section II. Microwave electrometry of the resonator mode, studies of the coherence times of the atom-resonator-field interaction and the atomic superposition states generated following the interaction with this resonator field, and high precision measurements of residual dc electric fields are then presented in Section III. In Section IV conclusions are drawn.

II. EXPERIMENT

The apparatus used in the experiments reported here has been described previously [29,30]. A pulsed supersonic beam of helium atoms in the metastable $1s2s\ ^3S_1$ level was generated in a dc electric discharge at the exit of a pulsed valve operated at a repetition rate of 50 Hz [32]. The beam, with a mean longitudinal speed of $v_z = 2000 \pm 50\ \text{m/s}$, was collimated and charged particles produced in the discharge were filtered out. It then entered a cryogenically cooled region in the apparatus maintained at a temperature of 3.8 K. In this region, the atoms were excited to the $1s55s\ ^3S_1$ ($|55s\rangle$) Rydberg level using the $1s2s\ ^3S_1 \rightarrow 1s3p\ ^3P_2 \rightarrow 1s55s\ ^3S_1$ two-color two-photon excitation scheme [33]. This was implemented using focused continuous wave (CW) laser radiation [$\sim 100\ \mu\text{m}$ Gaussian full width at half maximum (FWHM)], at wavelengths in the ultraviolet (UV) 388.975 nm, and infrared (IR) 786.817 nm, for each step, respectively. Rydberg state laser photoexcitation was performed at the beginning of each cycle of the experiment for times of $\tau_{\text{excite}} = 850$ or 2850 ns. This resulted in the generation of excited atoms in a steplike spatial distribution of length $L_{\text{Ry}} \simeq v_z \tau_{\text{excite}} = 1.7$ or 5.7 mm in the longitudinal dimension. The spatial distributions in the y and x dimensions were Gaussian with FWHMs of $\sim 100\ \mu\text{m}$ set by the focal spot size of, and Doppler selection by, the narrow bandwidth CW laser beams, respectively. The divergence of the distribution of Rydberg atoms was ~ 0.05 mrad.

After photoexcitation, the Rydberg atoms traveled for $12.5\ \mu\text{s}$ to the grounded end of a $\lambda/4$ NbN superconducting CPW resonator as depicted in Fig. 1. This L-shaped resonator was fabricated by depositing a 100-nm-thick NbN film (blue-filled region in Fig. 1) with a critical temperature $T_c = 12.1\ \text{K}$ on a silicon substrate (white region in Fig. 1) with a relative permittivity $\epsilon_r = 11.3$. The resonator had a total length of 6.335 mm, a center conductor width of $20\ \mu\text{m}$, and $10\text{-}\mu\text{m}$ -wide insulating gaps. The longer straight section of

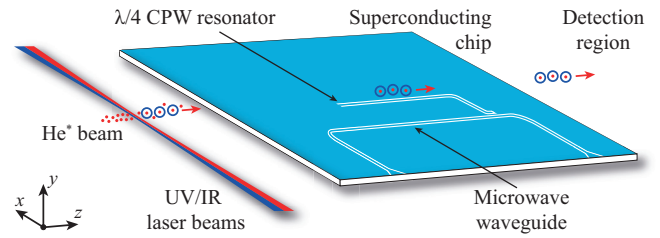


FIG. 1. Schematic diagram of the experimental apparatus. Note: Pairs of metallic electrodes that (i) surround the laser photoexcitation region, (ii) are located above the superconducting chip, and (iii) delineate the detection region are not shown. The filled blue regions (white regions) on the superconducting chip represent the NbN film (silicon substrate).

the resonator was aligned with the axis of propagation of the atomic beam.

The temperature of the superconducting chip was stabilized such that the third-harmonic frequency of the resonator was $\omega_3 = 2\pi \times 19.556\ \text{GHz}$. In this mode the quality factor was $Q \simeq 2500$ [30]. Pulses of microwave radiation at angular frequencies close to ω_3 were injected, at a time t_μ , into the resonator from a coplanar microwave waveguide (U-shaped structure on a superconducting chip in Fig. 1) to drive the single-color two-photon transition between the $|55s\rangle$ and the $1s56s\ ^3S_1$ ($|56s\rangle$) Rydberg levels. These levels have quantum defects of 0.296 669 29 and 0.296 668 83, respectively [34]. Consequently, the two-photon $|55s\rangle \rightarrow |56s\rangle$ transition occurs at $\omega_{55s,56s}/2 = 2\pi \times 19.556\ 499\ \text{GHz}$ in the absence of external fields. Their field-free fluorescence lifetimes are calculated to be 130 and 137 μs , respectively. Stray electric fields at the position of the atoms above the chip were compensated by applying pulsed electric potentials to a pair of metal electrodes (not shown in Fig. 1) that were located 10 mm above and parallel to the superconducting-chip surface. These potentials were switched on adiabatically to avoid population transfer to other Rydberg states as the atoms passed the edge of the chip closest to the excitation region and switched off adiabatically after the atoms crossed the chip.

The populations of the $|55s\rangle$ and $|56s\rangle$ Rydberg states were determined following state-selective pulsed electric-field ionization performed in a detection region located downstream in the apparatus from the superconducting chip. Electrons generated in this process were accelerated out from the cryogenic part of the apparatus to a microchannel plate detector operated at room temperature. Detection was implemented by single-event counting. The time dependence of the pulsed electric field used to ionize the Rydberg atoms was optimized to allow the time of flight of electrons produced following ionization of the $|55s\rangle$ state to be clearly distinguished from those from the $|56s\rangle$ state [30].

In general, the experiments were performed in a regime in which ~ 1 Rydberg atom crossed the superconducting chip per experimental cycle. In this mode of operation, perturbations arising from interactions between pairs atoms were minimized, and the detection probability of ~ 0.7 at the MCP was comparable for electrons originating from the $|55s\rangle$ and $|56s\rangle$ Rydberg states. For each set of measurement conditions,

between 400 and 500 cycles of the experiment were carried out to determine the corresponding Rydberg state populations.

III. RESULTS

In the experiments reported here, the Rydberg atoms were exploited to probe the spatial distribution of the microwave field and measure dc electric fields at the vacuum–solid-state interface above the CPW resonator. The amplitude of the oscillating electric component of the microwave field was determined from the Rabi frequency at which the two-photon $|55s\rangle \rightarrow |56s\rangle$ transition was driven. These measurements also allowed the coherence time of the atom–resonator–field interaction to be determined. Residual uncanceled dc electric fields close to the surface of the cryogenically cooled superconducting chip, and the coherence times of atomic superposition states generated following the interaction of the atoms with the resonator field, were measured by cavity-enhanced Ramsey spectroscopy.

A. Microwave field distribution

The L-shaped geometry of the $\lambda/4$ CWP resonator used in this work was chosen so that the straight section along which the beam of Rydberg atoms traveled had a length approximately equal to the wavelength of the microwave field in the third-harmonic mode. This is indicated schematically in Fig. 2(a). The red curve in the central part of this figure represents the microwave electric field at the surface of the superconducting chip. The spatial distribution of the microwave field surrounding the two electric-field maxima in this straight section of the resonator must be taken into consideration when performing time-domain measurements of the coherent interaction of the atoms with the microwave field in the resonator.

To measure the longitudinal microwave field distribution above the straight section of the resonator aligned with the axis of propagation of the atomic beam, Rydberg atoms in the $|55s\rangle$ state, in distributions for which $L_{\text{Ry}} = 1.7$ mm, were prepared by laser photoexcitation. A single microwave pulse with a duration $\tau_{\mu} = 50$ ns was then injected into the resonator at the frequency $\omega_{55s,56s}/2$. This pulse duration was chosen to be significantly shorter than the inverse of the maximal resonant Rabi frequency of $\sim 2\pi \times 3$ MHz encountered in these measurements. The time between laser photoexcitation to the $|55s\rangle$ state and the injection of this pulse was adjusted while the population of the $|56s\rangle$ state was monitored. The results of these measurements, performed for microwave pulse injection times between $t_{\mu} = 10$ and $17 \mu\text{s}$ are presented in Fig. 2(b). From these data it is seen that no population transfer to the $|56s\rangle$ state occurred when the microwave pulse was injected into the resonator before the atoms reach the grounded end closest to the laser photoexcitation region, i.e., for $t_{\mu} \lesssim 12 \mu\text{s}$. However, for longer time delays, population transfer was observed. This represented the average population transfer within the 1.7-mm-long distributions of the Rydberg atoms. There are two injection times, close to $t_{\mu} = 13$ and $15 \mu\text{s}$, for which significant population transfer occurs. These are the times when the excited atoms were located above electric-field maxima in the resonator mode when the microwave pulses

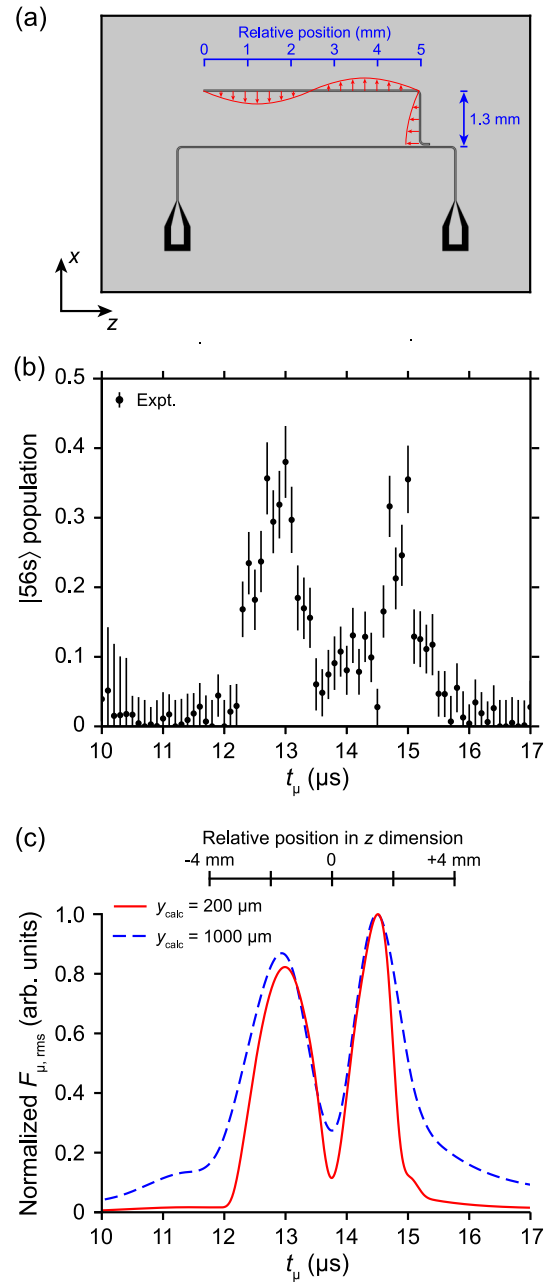


FIG. 2. (a) Schematic diagram of the superconducting chip with the microwave electric field in the third-harmonic mode of the L-shaped CPW resonator indicated in red. (b) Population transfer to the $|56s\rangle$ state measured as a function of the time between Rydberg-state laser photoexcitation, and the injection of a microwave pulse of duration $\tau_{\mu} = 50$ ns into the resonator at the frequency $\omega_{55s,56s}/2$. (c) The normalized calculated rms microwave electric field, $F_{\mu,\text{rms}}$, 200 μm (continuous red curve) and 1000 μm (dashed blue curve) above the resonator in the y dimension.

were applied. From the 2000 ± 50 m/s longitudinal speed of the beam of Rydberg atoms, the time interval of $\sim 2 \mu\text{s}$ between the two peaks in the experimental data in Fig. 2(b) corresponds to a 4-mm spatial separation between the maxima in the microwave field experienced by the atoms.

As seen from Fig. 2(a), when operated in its third-harmonic mode, the straight section of the CPW resonator over which

the atoms traveled has a length equal to approximately one wavelength of the microwave radiation at $\omega = 2\pi \times 19.556499$ GHz. Since the length of this section of the resonator is ~ 5 mm, the wavelength of the microwave field within the resonator, accounting for the effects of the relative permittivity of the bulk silicon substrate ($\epsilon_r = 11.3$) on which the CWP resonator was fabricated, the fabrication process, and the kinetic inductance of the NbN, is ~ 5 mm. Hence the spatial separation between the microwave field maxima within the resonator structure is ~ 2.5 mm.

The vacuum wavelength of microwave radiation with an angular frequency of $\omega = 2\pi \times 19.556499$ GHz is 15.3 mm. In the near-field region $< 1000 \mu\text{m}$ above the chip surface where the atoms were located in the experiments, the spatial separation between the microwave electric-field maxima lies between the solid-state and the vacuum half-wavelengths. The normalized root-mean-square (rms) microwave electric-field distribution, $F_{\mu, \text{rms}}$, calculated for distances $y_{\text{calc}} = 200$ and $1000 \mu\text{m}$ directly above the center conductor in the long straight section of the resonator, is displayed as the continuous red and dashed blue curves in Fig. 2(c), respectively. These electric-field distributions were calculated using finite element methods in CST Studio Suite [35], accounting for the dielectric properties of the superconducting chip. The asymmetry in each is a consequence of the presence of the perpendicular section of the resonator that approaches the U-shaped microwave waveguide at the end furthest from the laser photoexcitation region [see Fig. 2(a)]. Interference between the field in the resonator and the traveling microwave field in the waveguide gives rise to a small asymmetry in the field distributions in the x dimension on either side of the resonator. However, under the experimental conditions, contributions from the strongly enhanced field in the resonator are dominant. From the data in Fig. 2(a), it is seen that the calculated separation between the electric-field maxima at distances $< 1000 \mu\text{m}$ above the surface of the chip is in good qualitative agreement with the experimental observations. However, the changes in the form of these distributions with distance above the superconducting chip are not sufficient to allow the typical atom-surface distance in the experiments to be inferred directly from them.

The deviations of the experimental data from the general form of the calculated microwave field distribution near the second maximum between $t_\mu = 14$ and $15 \mu\text{s}$ originate from a combination of defects or adsorbates on the surface of the resonator, small misalignments between the Rydberg atom beam and the resonator, and effects of interference with the microwave field scattered from the copper electrodes surrounding the superconducting chip. We expect that in the future steps can be taken to improve control over these aspects of the experiment. These will include, for example, the use of inhomogeneous electric fields generated above chip-based electrode structures to guide the Rydberg atoms directly over the resonator [36].

B. Coherent atom-resonator-field interactions

The coherence times of the atom-resonator-field interaction were determined by time-domain measurements of Rabi oscillations presented in Fig. 3. When recording the

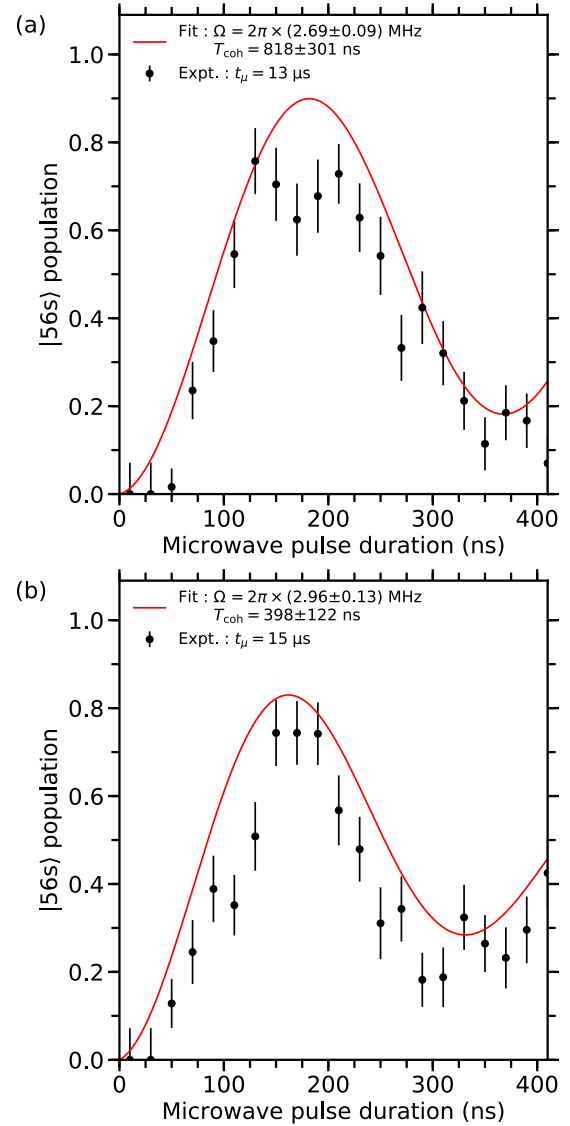


FIG. 3. Rabi oscillations in the population of the $|56s\rangle$ state (black points) recorded by injecting pulses of microwave radiation at the frequency $\omega_{55s,56s}/2$ into the CPW resonator at times of (a) $t_\mu = 13 \mu\text{s}$ and (b) $t_\mu = 15 \mu\text{s}$. The continuous red curve in each panel represents a least-squares fit of the expression in Eq. (1) from which the Rabi frequencies and coherence times indicated were obtained.

data in this figure, the resonator was driven on resonance with the field-free atomic transition frequency at $\omega_{55s,56s}/2 = 19.556499$ GHz. These data were obtained with microwave pulses injected into the resonator at two different times after Rydberg state photoexcitation, i.e., two different values of t_μ . The results of measurements made by monitoring the population of the $|56s\rangle$ state, while adjusting the duration of the microwave pulse injected into the resonator at $t_\mu = 13 \mu\text{s}$, are displayed in Fig. 3(a). At the time when this microwave pulse was applied the Rydberg atoms were located close to the position of the first electric-field maximum they encountered in the resonator mode [see Fig. 2(b)]. The Rabi frequency, Ω , and the coherence time, T_2 , were obtained by fitting the

function

$$P_{56s}(t) = [1 - \cos(\Omega t) e^{-t/T_2}]/2, \quad (1)$$

describing the time evolution of a pure two-level system driven on resonance with exponential damping (red curve) to the experimental data. For the data in Fig. 3(a), $\Omega = 2\pi \times 2.69 \pm 0.09$ MHz and $T_2 = 818 \pm 301$ ns.

The coherence time of the interaction of the atoms with the microwave field close to the second electric-field maximum of the resonator mode was determined in a similar way. In this case the time delay between Rydberg state photoexcitation and the injection of the microwave pulse into the resonator was increased to $t_\mu = 15 \mu\text{s}$, i.e., close to the second maximum in the $|56s\rangle$ population in Fig. 2(b). The Rabi frequency obtained by fitting the expression in Eq. (1) to these data was $\Omega = 2\pi \times 2.96 \pm 0.13$ MHz and the coherence time was $T_2 = 398 \pm 122$ ns [red curve in Fig. 3(b)]. The coherence time at this second interaction position is shorter than that observed close to the first microwave field maximum. This indicates that inhomogeneities in the residual uncanceled dc electric fields and the microwave field distribution above the resonator are greater than at the first position.

In general, the coherence times of the atom–resonator–field interaction observed in these and earlier experiments at hybrid Rydberg-atom–superconducting-circuit interfaces reduce as the Rabi frequency increases [29–31]. This indicates that the decoherence observed, for example, in the data in Fig. 3, is a consequence of dephasing of the atom–field interaction across the ensemble of excited atoms. Since the Rydberg atoms were distributed over a region with a length of ~ 1.7 mm in the z dimension and widths of $\sim 100 \mu\text{m}$ in the x and y dimensions when they interacted with the inhomogeneous microwave field above the resonator, those at different positions coupled to the resonator field with different Rabi frequencies. Dephasing of the oscillatory population transfer between the Rydberg states at this range of Rabi frequencies then leads to the decoherence observed in the data in Fig. 3. For stronger driving, the measured Rabi frequency increases. However, this also results in larger differences in the Rabi frequencies across the ensemble of atoms and hence more rapid dephasing and shorter measured coherence times. The data in Fig. 3 are commensurate with a distribution of Rabi frequencies that varies by $\pm 15\%$ about the mean and therefore within the range of Rabi frequencies expected under the experimental conditions.

The single-color two-photon $|55s\rangle \rightarrow |56s\rangle$ transition employed in this work may be considered to follow an off-resonant pathway through the $1s55p \ ^3P_J$ levels ($|55p\rangle$). Since the virtual intermediate state in this two-photon scheme is detuned by $\Delta = 2\pi \times 10.437931$ GHz from these levels (the quantum defects of the $1s55p \ ^3P_J$ levels are ~ 0.068354 [34]), and the 3P_J fine structure at $n = 55$ in helium is $\sim 2\pi \times 1.2$ MHz [34,37], the electric dipole transition moments associated with the single-photon $|55s\rangle \rightarrow |55p\rangle$ and $|55p\rangle \rightarrow |56s\rangle$ transitions, $\mu_{55s,55p} = 2457 e a_{\text{He}}$ and $\mu_{55p,56s} = 1185 e a_{\text{He}}$ (e is the electron charge, and a_{He} is the Bohr radius corrected for the reduced mass of helium), respectively, were calculated using the Numerov method neglecting the fine structure. In this situation, the two-photon Rabi frequency, $\Omega_{55s,56s}$, depends on the product of two single-photon Rabi frequencies, $\Omega_{55s,56s} = F_\mu \mu_{55s,55p}/\hbar$ and

$\Omega_{55p,56s} = F_\mu \mu_{55p,56s}/\hbar$, where F_μ is the amplitude of the microwave field, and the detuning Δ from the intermediate state such that on two-photon resonance [38]

$$\Omega_{55s,56s} = \frac{\Omega_{55s,55p} \Omega_{55p,56s}}{2\Delta}. \quad (2)$$

Using the values of the transition dipole moments listed above, together with the measured Rabi frequencies of $\sim 2\pi \times 2.5$ MHz in Fig. 3, the amplitude of the microwave electric field at the position of the atoms in the experiments was determined to be $F_\mu = 0.11$ V/cm. This is consistent with the microwave field of ~ 0.1 V/cm at a distance $300 \mu\text{m}$ above the surface of the CPW resonator that was estimated by accounting for the 15.8 mW output power from the microwave source, the 22.5 dB attenuation between the source and the waveguide on the superconducting chip, and the characteristics of the resonator that yield an estimated steady-state circulating microwave power in the resonator of ~ 5 mW [39].

The data presented in Fig. 3 were recorded with short distributions of Rydberg atoms, i.e., $L_{\text{Ry}} \simeq 1.7$ mm, under conditions in which typically only one atom interacted with the resonator field per experimental cycle. To characterize effects arising from a greater number of atoms interacting at a time with the microwave field in the single resonator mode, longer distributions of atoms were prepared by increasing the time during which laser photoexcitation was performed, from $\tau_{\text{excite}} = 850$ to 2850 ns. Rabi oscillations in the population of the $|56s\rangle$ state recorded under these different conditions, when the center of the distribution of excited atoms was located close to the first microwave field maximum in the resonator mode, are presented in Fig. 4(a). It can be seen from these data that in the measurement performed with the longer distribution of atoms, i.e., for $L_{\text{Ry}} \simeq 5.7$ mm (open red triangles), the contrast of the Rabi oscillations, and the coherence time of the atom–resonator–field interaction, are reduced compared to the case in which $L_{\text{Ry}} \simeq 1.7$ mm (filled blue circles). These observations are consistent with decoherence arising as a result of dephasing across the ensemble of excited atoms. In the inhomogeneous microwave field above the resonator, ensembles of atoms with a broader spatial distribution experience a wider range of microwave field strengths and hence couple to the resonator field with a wider range of Rabi frequencies. This wider range of Rabi frequencies gives rise to more rapid dephasing. The continuous and dashed curves in Fig. 4(a) were obtained by fitting the expression in Eq. (1) to the experimental data recorded for $\tau_{\text{excite}} = 850$ and 2850 ns as indicated. This function does not accurately describe the experimental data recorded with the longer distribution of atoms. This leads to the conclusion that because of the inhomogeneity of the microwave field above the resonator, the atom–resonator–field interaction can only be described as being comparable to that of a two-level system driven on resonance with exponential damping when short distributions of Rydberg atoms that remain well localized as they fly across the superconducting chip are employed.

Further information on the effect of changing the size of the distribution of excited atoms, and hence the number of atoms prepared in each experimental cycle, on the atom–resonator–field interaction was obtained from the Fourier transforms of the experimental data in Fig. 4(a). The magnitudes of the

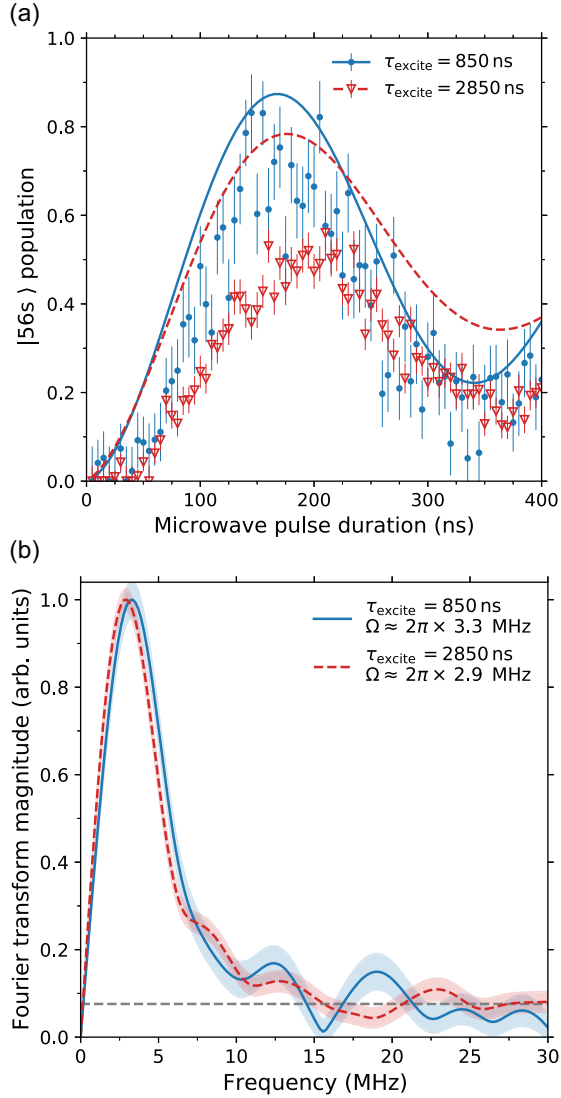


FIG. 4. (a) Rabi oscillations in the population of the $|56s\rangle$ state recorded by injecting pulses of microwave radiation at the frequency $\omega_{55s,56s}/2$ into the CPW resonator when $t_\mu = 13 \mu s$. Measurements made following short ($\tau_{\text{excite}} = 850$ ns) and long ($\tau_{\text{excite}} = 2850$ ns) periods of laser photoexcitation and hence with short ($L_{\text{Ry}} = 1.7$ mm), and long ($L_{\text{Ry}} = 5.7$ mm) distributions of Rydberg atoms are indicated by the filled circles and open triangles, respectively. (b) Fourier transforms of the experimental data in (a). The dashed gray line in (b) represents the level of the background fluctuations in the Fourier transform of the experimental data.

Fourier transforms of the data recorded for $\tau_{\text{excite}} = 850$ and 2850 ns are represented by the continuous blue and dashed red curves in Fig. 4(b), respectively. The maxima in these Fourier transforms both lie close to 3 MHz. For the shorter distribution of atoms, the peak occurs at 3.1 MHz, while for the longer distribution it occurs at 2.7 MHz. Since the longer distributions of Rydberg atoms in these experiments contain larger numbers of excited atoms, it may be expected that effects arising from collective coupling of the atoms to the resonator field could become apparent. Collective effects

would, in the simplest case, result in an increase in the observed Rabi frequency by a factor of \sqrt{N} , where N is the number of atoms, when compared with that associated with the interaction of a single atom. In the data in Fig. 4(b) that were recorded with the longer distribution of atoms, no notable features are observed close to \sqrt{N} multiples of the fundamental oscillation frequency. In addition, no broadening of the spectral profile toward higher frequencies is seen. This suggests that collective effects do not play a significant role under the current experimental conditions. Because the number of Rydberg atoms prepared in each experimental cycle is typically between 1 and 3 in the longer distributions prepared, for situations in which two atoms couple simultaneously to the resonator field, the probability of both being located within the inhomogeneous microwave field distribution at positions of similar field strength is low. Pairs of atoms are therefore unlikely to couple with equal Rabi frequencies to the resonator field, and no significant collective enhancement in the measured Rabi frequency will be observed. The possibility of observing collective effects is also limited in the present apparatus because of the comparatively short photon residence time (< 100 ns) in the resonator.

C. Cavity-enhanced Ramsey spectroscopy

The coherence time of the atom–resonator–field interaction that arises because of the inhomogeneity of the microwave field distribution can be distinguished from the coherence times of the atomic superposition states generated following the interaction of the atoms with the resonator field. The latter can be inferred from cavity-enhanced Ramsey spectra. To achieve this, Ramsey spectra were recorded with pairs of 50-ns duration microwave pulses injected into the resonator. The first of these pulses was applied at time $t_\mu = 13 \mu s$, and the time interval between the two pulses was set to $2 \mu s$. This resulted in Ramsey fringes for the two-photon $|55s\rangle \rightarrow |56s\rangle$ transition with a periodicity of 250 kHz. A Ramsey spectrum recorded by scanning the microwave frequency across the atomic transition is displayed in Fig. 5. The experimental data in this figure are indicated by the filled black points. The continuous red curve represents a calculated spectrum obtained by considering the time evolution of the microwave field in the resonator mode and the population transfer between the atomic states. The theoretical model and numerical methods used in these calculations are described in detail in Ref. [30]. The calculated spectrum was fit to the experimental data with the atomic transition frequency and the coherence time of the atomic superposition states chosen as the free fit parameters.

The highest precision determination of the atomic transition frequency and the coherence time of the atomic superpositions states were obtained from a Ramsey spectrum similar to that in Fig. 5 but recorded over a narrower frequency range with smaller frequency steps between measurements. This second spectrum is displayed as the filled black points in Fig. 6. The quantitative agreement of the function fit to this experimental data with the results of the measurements demonstrates the suitability of the fitting procedure used to determine the atomic transition frequency and the high fringe visibility resulting from the extended coherence times of the atomic superposition states during the free-evolution

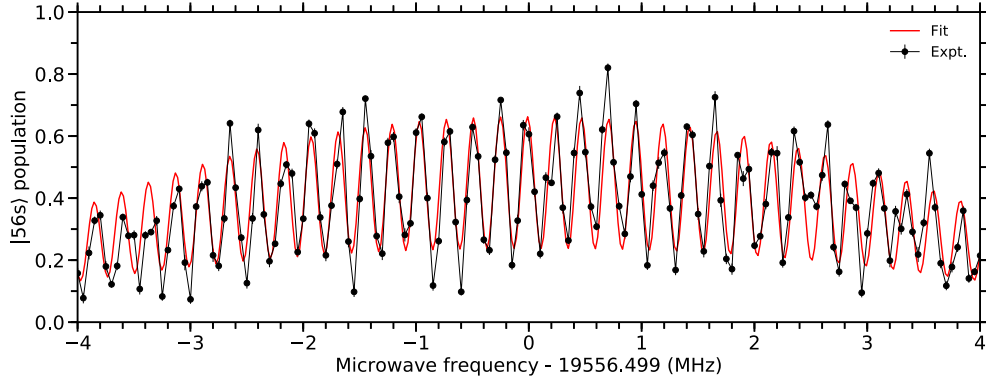


FIG. 5. Cavity-enhanced Ramsey spectrum of the $|55s\rangle \rightarrow |56s\rangle$ transition in helium. The experimental data are indicated by the filled black points. A calculated spectrum in which the time dependence of the microwave field in the resonator was accounted for before fitting to the experimental data is indicated by the continuous red curve (see text for details).

time in the Ramsey sequence. From the fit to the data in Figs. 5 and 6 (continuous red curves) and additional single pulse Rabi spectra of the kind reported in Ref. [29] that were recorded to aid in the identification of the Ramsey-fringe closest to resonance, an atomic transition frequency of $2\pi \times (19.5564506 \pm 0.0000023)$ GHz was obtained. This is $2\pi \times 48.4$ kHz below the field-free two-photon transition frequency of $\omega_{55s,56s}/2 = 2\pi \times 19.556499$ GHz. This deviation from the field-free transition frequency is attributed to the effect of a weak residual uncanceled stray electric field at the position of the atoms close to the cryogenically cooled superconducting chip surface. The $|55s\rangle \rightarrow |56s\rangle$ transition between the triplet states in helium exhibits a quadratic Stark

shift toward lower frequencies in weak electric fields [29]. From the calculated Stark effect for this transition, the stray electric field required to cause a $-2\pi \times (48.4 \pm 2.3)$ kHz shift in the two-photon transition frequency was determined to have a magnitude of 26.6 ± 0.6 mV/cm. From these data and the results presented in Section III A, it is concluded that this represents the residual uncanceled stray dc electric field 300 μm above the cryogenically cooled superconducting CPW resonator. The fit to the spectrum in Fig. 6 yielded a coherence time of the atomic superposition states, in the period of free evolution between the Ramsey pulses, of ~ 2.5 μs . This corresponds to the flight time of the atoms over the 5-mm-long straight section of the resonator. Since the Rydberg states used in this work have fluorescence lifetimes in excess of 100 μs , it is expected that this coherence time could be extended if more slowly moving or stationary atoms were employed.

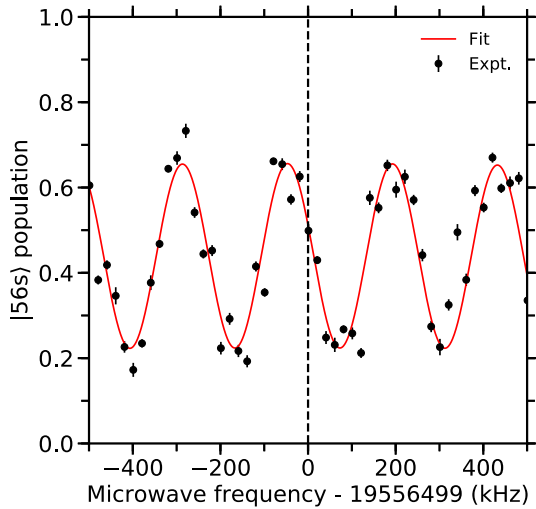


FIG. 6. A section of the cavity enhanced Ramsey spectrum recorded under the same experimental conditions as that in Fig. 5 but with measurements performed at smaller frequency intervals (filled black points). The calculated spectrum, fit to the experimental data to determine the atomic transition frequency of $2\pi \times (19.5564506 \pm 0.0000023)$ GHz and coherence time the atomic superposition states of ~ 2.5 μs in the absence of the microwave field, is indicated by the continuous red curve.

IV. CONCLUSIONS

In conclusion, by performing time-domain measurements of population transfer between the $1s55s$ 3S_1 and the $1s56s$ 3S_1 Rydberg levels in helium atoms traveling over a $\lambda/4$ CPW superconducting microwave resonator, the electric-field distribution of a single resonator mode was characterized. These results demonstrate the effect of the dielectric properties at the vacuum–solid-state interface on the microwave field distribution at the position of the atoms. Comparison of these time-domain measurements of Rabi oscillations with cavity-enhanced Ramsey spectra recorded in the frequency domain, have allowed the coherence times associated with the atom–resonator-field interaction and the coherence times of the atomic superposition states generated through the interaction with the resonator field to be distinguished. The atomic coherence times were limited to ~ 2.5 μs in the present work by the flight time of the Rydberg atoms across the CPW resonator. This coherence time could be extended by preparing samples of more slowly moving or stationary atoms. The observation of coherence times in excess of 1 μs , together with spatially resolved characterization of the microwave field in the resonator mode and the control over stray electric fields that were reduced to 26.6 ± 0.6 mV/cm at a distance

of $300\ \mu\text{m}$ above the superconducting chip surface, represent major developments in the realization of hybrid quantum systems comprising Rydberg atoms and superconducting microwave circuits for applications in quantum information processing. These advances have benefited from the use of a $\lambda/4$ CPW resonator geometry and helium atoms to minimize effects of stray electric fields arising as a result of surface adsorption.

ACKNOWLEDGMENTS

This work was supported by the European Research Council (ERC) under the European Union's Horizon 2020 research and innovation program (Grant No. 683341) and the Engineering and Physical Sciences Research Council (EPSRC) through the EPSRC Centre for Doctoral Training in Delivering Quantum Technologies.

-
- [1] T. F. Gallagher, *Rydberg Atoms* (Cambridge University Press, Cambridge, England, 1994).
- [2] J. M. Raimond, M. Brune, and S. Haroche, Manipulating quantum entanglement with atoms and photons in a cavity, *Rev. Mod. Phys.* **73**, 565 (2001).
- [3] H. Walther, B. T. H. Varcoe, B. Englert, and T. Becker, Cavity quantum electrodynamics, *Rep. Prog. Phys.* **69**, 1325 (2006).
- [4] R. G. Hulet, E. S. Hilfer, and D. Kleppner, Inhibited Spontaneous Emission by a Rydberg Atom, *Phys. Rev. Lett.* **55**, 2137 (1985).
- [5] M. Brune, F. Schmidt-Kaler, A. Maali, J. Dreyer, E. Hagley, J. M. Raimond, and S. Haroche, Quantum Rabi Oscillation: A Direct Test of Field Quantization in a Cavity, *Phys. Rev. Lett.* **76**, 1800 (1996).
- [6] S. Gleyzes, S. Kuhr, C. Guerlin, J. Bernu, S. Deléglise, U. Busk Hoff, M. Brune, J. M. Raimond, and S. Haroche, Quantum jumps of light recording the birth and death of a photon in a cavity, *Nature (London)* **446**, 297 (2007).
- [7] A. Wallraff, D. I. Schuster, A. Blais, L. Frunzio, R.-S. Huang, J. Majer, S. Kumar, S. M. Girvin, and R. J. Schoelkopf, Strong coupling of a single photon to a superconducting qubit using circuit quantum electrodynamics, *Nature (London)* **431**, 162 (2004).
- [8] A. Blais, A. L. Grimsmo, S. M. Girvin, and A. Wallraff, Circuit quantum electrodynamics, *Rev. Mod. Phys.* **93**, 025005 (2021).
- [9] P. Rabl, D. DeMille, J. M. Doyle, M. D. Lukin, R. J. Schoelkopf, and P. Zoller, Hybrid Quantum Processors: Molecular Ensembles as Quantum Memory for Solid State Circuits, *Phys. Rev. Lett.* **97**, 033003 (2006).
- [10] S. D. Hogan, J. A. Agner, F. Merkt, T. Thiele, S. Filipp, and A. Wallraff, Driving Rydberg-Rydberg Transitions from a Coplanar Microwave Waveguide, *Phys. Rev. Lett.* **108**, 063004 (2012).
- [11] M. Kiffner, A. Feizpour, K. T. Kaczmarek, D. Jaksch, and J. Nunn, Two-way interconversion of millimeter-wave and optical fields in Rydberg gases, *New J. Phys.* **18**, 093030 (2016).
- [12] B. T. Gard, K. Jacobs, R. McDermott, and M. Saffman, Microwave-to-optical frequency conversion using a cesium atom coupled to a superconducting resonator, *Phys. Rev. A* **96**, 013833 (2017).
- [13] J. Han, T. Vogt, C. Gross, D. Jaksch, M. Kiffner, and W. Li, Coherent Microwave-To-Optical Conversion Via Six-Wave Mixing in Rydberg Atoms, *Phys. Rev. Lett.* **120**, 093201 (2018).
- [14] D. Petrosyan, K. Mølmer, J. Fortágh, and M. Saffman, Microwave to optical conversion with atoms on a superconducting chip, *New J. Phys.* **21**, 073033 (2019).
- [15] K. R. Patton and U. R. Fischer, Ultrafast Quantum Random Access Memory Utilizing Single Rydberg Atoms in a Bose-Einstein Condensate, *Phys. Rev. Lett.* **111**, 240504 (2013).
- [16] L. Sárkány, J. Fortágh, and D. Petrosyan, Faithful state transfer between two-level systems via an actively cooled finite-temperature cavity, *Phys. Rev. A* **97**, 032341 (2018).
- [17] J. D. Pritchard, J. A. Isaacs, M. A. Beck, R. McDermott, and M. Saffman, Hybrid atom-photon quantum gate in a superconducting microwave resonator, *Phys. Rev. A* **89**, 010301(R) (2014).
- [18] L. Sárkány, J. Fortágh, and D. Petrosyan, Long-range quantum gate via Rydberg states of atoms in a thermal microwave cavity, *Phys. Rev. A* **92**, 030303(R) (2015).
- [19] K.-Y. Liao, Z.-T. Liang, J. Liang, W. Huang, and Y.-X. Du, Hybrid superconductor-atom quantum interface with Raman chirped shortcut to adiabatic passage *Opt. Express* **27**, 29639 (2019).
- [20] S. Garcia, M. Stammeier, J. Deiglmayr, F. Merkt, and A. Wallraff, Single-Shot Nondestructive Detection of Rydberg-Atom Ensembles by Transmission Measurement of a Microwave Cavity, *Phys. Rev. Lett.* **123**, 193201 (2019).
- [21] G. Calajó and P. Rabl, Strong coupling between moving atoms and slow-light Cherenkov photons, *Phys. Rev. A* **95**, 043824 (2017).
- [22] H. Hattermann, M. Mack, F. Karlewski, F. Jessen, D. Cano, and J. Fortágh, Detrimental adsorbate fields in experiments with cold Rydberg gases near surfaces, *Phys. Rev. A* **86**, 022511 (2012).
- [23] C. Hermann-Avigliano, R. C. Teixeira, T. L. Nguyen, T. Cantat-Moltrecht, G. Nogues, I. Dotsenko, S. Gleyzes, J. M. Raimond, S. Haroche, and M. Brune, Long coherence times for Rydberg qubits on a superconducting atom chip, *Phys. Rev. A* **90**, 040502(R) (2014).
- [24] T. Thiele, J. Deiglmayr, M. Stammeier, J.-A. Agner, H. Schmutz, F. Merkt, and A. Wallraff, Imaging electric fields in the vicinity of cryogenic surfaces using Rydberg atoms, *Phys. Rev. A* **92**, 063425 (2015).
- [25] L. A. Jones, J. D. Carter, and J. D. D. Martin, Rydberg atoms with a reduced sensitivity to dc and low-frequency electric fields, *Phys. Rev. A* **87**, 023423 (2013).
- [26] D. W. Booth, J. Isaacs, and M. Saffman, Reducing the sensitivity of Rydberg atoms to dc electric fields using two-frequency ac field dressing, *Phys. Rev. A* **97**, 012515 (2018).
- [27] A. A. Morgan, V. Zhelyazkova, and S. D. Hogan, Preparation of circular Rydberg states in helium with $n \geq 70$ using a modified version of the crossed-fields method, *Phys. Rev. A* **98**, 043416 (2018).
- [28] M. Peper, J. Deiglmayr, F. Merkt, C. Sanna, and H. B. v. L. van den Heuvel, Magic Rydberg-Rydberg transitions in electric fields, *Phys. Rev. A* **100**, 032512 (2019).
- [29] A. A. Morgan and S. D. Hogan, Coupling Rydberg Atoms to Microwave Fields in a Superconducting Coplanar Waveguide Resonator, *Phys. Rev. Lett.* **124**, 193604 (2020).

- [30] D. M. Walker, A. A. Morgan, and S. D. Hogan, Cavity-enhanced Ramsey spectroscopy at a Rydberg-atom-superconducting-circuit interface, *Appl. Phys. Lett.* **117**, 204001 (2020).
- [31] M. Kaiser, C. Glaser, L. Y. Ley, J. Grimm, H. Hattermann, D. Bothner, D. Koelle, R. Kleiner, D. Petrosyan, A. Günther, J. Fortágh, Cavity driven Rabi oscillations between Rydberg states of atoms trapped on a superconducting atom chip, [arXiv:2105.05188](https://arxiv.org/abs/2105.05188) (2021).
- [32] T. Halfmann, J. Koensgen, and K. Bergmann, A source for a high-intensity pulsed beam of metastable helium atoms, *Meas. Sci. Technol.* **11**, 1510 (2000).
- [33] S. D. Hogan, Y. Houston, and B. Wei, Laser photoexcitation of Rydberg states in helium with $n > 400$, *J. Phys. B: At. Mol. Opt. Phys.* **51**, 145002 (2018).
- [34] G. W. F. Drake, High precision theory of atomic helium, *Phys. Scr. T* **83**, 83 (1999).
- [35] CST Studio Suite, Dassault Systèmes, Vélizy-Villacoublay, France (2020).
- [36] P. Lancuba and S. D. Hogan, Guiding Rydberg atoms above surface-based transmission lines, *Phys. Rev. A* **88**, 043427 (2013).
- [37] A. Deller and S. D. Hogan, Microwave spectroscopy of the $1snp^3P_j$ fine structure of high Rydberg states in ^4He , *Phys. Rev. A* **97**, 012505 (2018).
- [38] T. R. Gentile, B. J. Hughey, D. Kleppner, and T. W. Ducas, Experimental study of one- and two-photon Rabi oscillations, *Phys. Rev. A* **40**, 5103 (1989).
- [39] J. M. Sage, V. Bolkhovsky, W. D. Oliver, B. Turek, and P. B. Welander, Study of loss in superconducting coplanar waveguide resonators, *J. Appl. Phys.* **109**, 063915 (2011).